Electronic Supplementary Material (ESI) for Chemical Communications.
This journal is © The Royal Society of Chemistry 2024

Electronic Supporting Information for:

Red-Light Operable Photosensitizer with Symmetry-Breaking Charge Transfer Induced Intersystem Crossing for Polymerization of Methyl Methacrylate

Zafar Mahmood,[a] *Shuqing Cai,*[a] *Noreen Rehmat*,[a] *Mariangela Di Donato,*[c] *Jianzhang Zhao*,*[b]

Shanshan Sun,[d] *Mingde Li,*[d] *Yanping Huo,*[a] *Shaomin Ji*,*[a]

[a] School of Chemical Engineering and Light Industry, Guangdong University of Technology，510006，P.R. China. E-mail: smji@gdut.edu.cn

[b] State Key Laboratory of Fine Chemicals, School of Chemical Engineering, Dalian University of Technology, E-208 West Campus, 2 Ling-Gong Road, Dalian 116024, P. R. China E-mail: zhaojzh@dlut.edu.cn

[c] LENS (European Laboratory for Non-Linear spectroscopy), Via N. Carrara1, I-50019 Sesto Fiorentino, Italy. E-mail: didonato@lens.unifi.it

[d] Department of Chemistry and Key Laboratory for Preparation and Application of Ordered Structural Materials of Guangdong Province, Shantou University, Shantou, 515063, P. R. China. E-mail: mdli@stu.edu.cn

Contents

1. General information

All the chemicals used in synthesis are analytical pure and were used as received. Solvents were dried and distilled before used for synthesis. ^{1}H and ^{13}C NMR were recorded on a 400 MHz AVANCE III HD 400 spectrometer and chemical shifts are reported in parts per million (ppm) relative to TMS, with the residual solvent peak used as an internal reference. The mass spectra were measured by TOF MS MALDI and ESI spectrometer.

Cyclovoltametric Measurement

The cyclic voltammetry curves were measured with the PGSTAT302N electrochemical workstation (Metrohm, Netherlands) in N_2 purged saturated dichloromethane solutions containing 0.10 M Bu_4NPF_6 as a supporting electrolyte and 0.5 mM bis(dipyrrin) complex or bodipy derivative. The counter electrode is a platinum electrode, a glassy carbon electrode is a working electrode, and the Ag/AgCl couple as the reference electrode. A ferrocenium/ferrocene (Fc^+/Fc) redox couple was used as an internal reference.

Singlet Oxygen Quantum Yield

The singlet oxygen of the compounds was measured using 1,3-Diphenylisobenzofuran (DPBF) as $^{1}O_2$ scavenger. The $^{1}O_2$ production was monitored by following the absorbance of DPBF at 414 nm. To determine the singlet oxygen quantum yield (Φ_Δ), a relative method was used according to the following equation. Methylene blue was used as standard (Φ_{Std} = 0.57, in DCM).

$$\phi_{\Delta,\mathrm{sam}} = \phi_{\Delta,std}\left(\frac{1-10^{A_{std}}}{1-10^{A_{sam}}}\right)\left(\frac{m_{sam}}{m_{std}}\right)\left(\frac{\eta_{sam}}{\eta_{std}}\right)^2 \qquad \text{(Eq. 1)}$$

Nanosecond Transient Absorption Spectroscopy

The nanosecond transient absorption spectra were acquired on LP980 laser flash photolysis spectrometer (Edinburg Instruments, UK). The signal was digitized with a Tektronix TDS 3012B oscilloscope. TTA delayed fluorescence of the compounds was also measured on a LP980 laser flash photolysis spectrometer using emission mode, excitd with an OpoletteTM 355II+UV nanosecond pulsed laser (OPOTEK, USA). The wavelength is tunable in the range 210-2200 nm. The samples were deaerated with N_2 for 15 min prior to investigations. The data were processed by LP900 software.

Femtosecond Transient Absorption Spectroscopy

The fs-TA spectra were measured using a femtosecond regenerative amplified Ti: sapphire laser system, as previously described in the literature.[1] The laser probe pulse was produced by utilizing 12.5% of the amplified 800 nm laser pulses to generate a white-light continuum (320−680 nm) by a CaF_2 crystal. Then, this probe beam was split into two parts before traversing the sample. One probe beam passed through the sample, while the other probe laser beam passed through the reference spectrometer to monitor the fluctuations of the probe beam intensity. The sample was excited by a 500 nm pulsed laser. The sample solutions were excited in a 2 mm path-length cuvette with a stirring bar.The recorded kinetic traces and transient spectra have been analyzed by using a global-analysis procedure.[2] The number of kinetic components has been estimated by performing a preliminary singular values decomposition (SVD) analysis.[3] Global analysis was performed using the GLOTARAN package (http://glotaran.org),[4] employing a linear uni-directional ("sequential") model.

2. Synthesis and Molecular structure characterization data

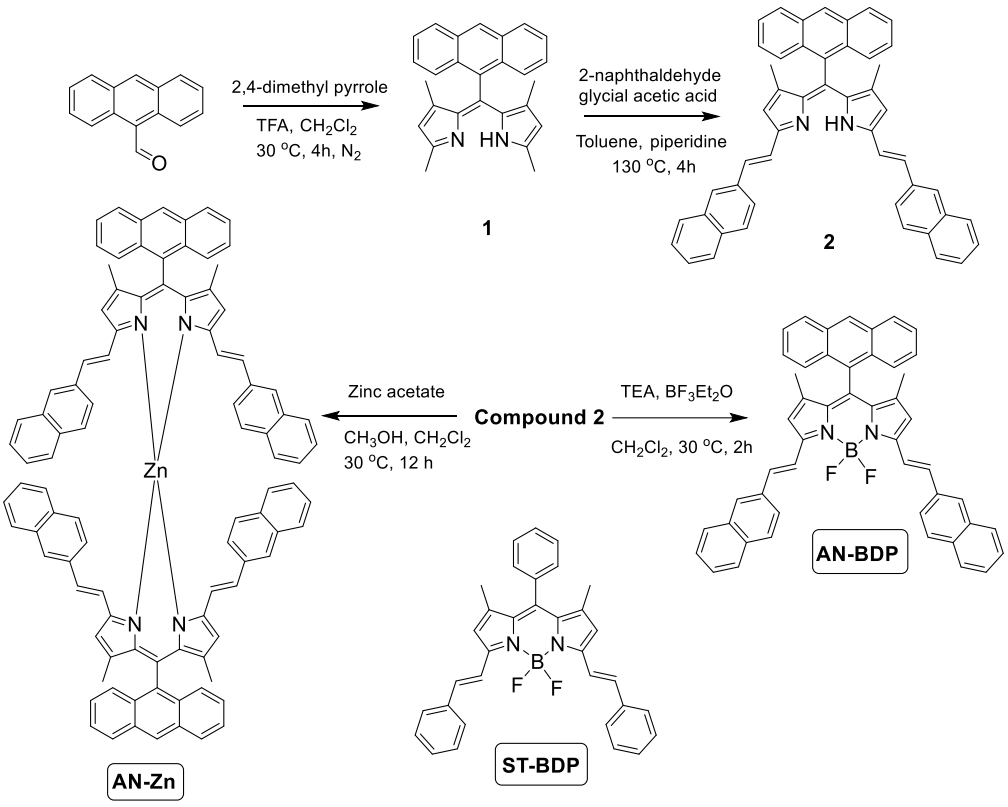

Scheme S1. Synthesis route of Zinc bis(dipyrrin) complex and reference BDP derivative.

Compounds 1 and 2 were prepared according to literature method.[1,5] Compound 1: ^{1}H NMR ($CDCl_3$, 400 MHz); δ 8.53 (s, 1H), 8.03–7.99 (m, 4H), 7.47–7.44 (m, 2H), 7.39–7.36 (m, 2H), 5.78 (s, 2H), 2.42 (s, 6H), 0.52 (s, 6H). ESI−HRMS Calcd for ($C_{27}H_{24}N_2$+H^+): *m/z* = 377.2018. Found: *m/z* = 377.2017. **Compound 2:** ^{1}H NMR ($CDCl_3$, 400 MHz); δ 8.58 (s, 1H), 8.07–8.04 (m, 4H), 7.90–7.85 (m, 8H), 7.71 (d, 2H, *J* = 8.0 Hz), 7.50–7.40 (m, 12H), 6.33 (s, 2H), 0.64 (s, 6H). ESI-HRMS ($C_{49}H_{36}N_2$+H^+) Calcd: *m/z* = 653.2957. Found: *m/z* = 653.2953.

Compounds AN-Zn, and AN-BDP were prepared following literature method with slight modifications.[5]

Synthesis of compound AN-Zn. Under N_2 atmosphere, 5 mL solution of zinc acetate (10 mg, 0.05 mmol. 1 equiv) in methanol was slowly added to the solution of compound 2 (65 mg, 0.1 mmol, 2 equiv) in 10 mL dry dichloromethane. After stirring the mixture at rt for overnight, the amount of solvent was reduced under reduced pressure and filtered. The precipitates was collected and rinsed thoroughly with methanol. The crude product was further purified with column chromatography (Silica gel, CH_2Cl_2/petroleum ether, 1/2, v/v) to give dark blue solid (50 mg, yield: 73 %). ^{1}H NMR ($CDCl_3$, 400 MHz); δ 8.56 (s, 2H), 7.96–7.91 (m, 8H), 7.62–7.57 (m, 12H), 7.38–7.26 (m, 24H), 7.06–7.03 (m, 4H), 6.69 (s, 4H), 6.49–6.45 (m, 4H), 0.72 (s, 12H). ^{13}C NMR (100 MHz, $CDCl_3$); δ 156.88, 144.32, 140.31, 140.04, 134.95, 133.60, 133.53, 133.37, 133.10, 131.39, 131.14, 128.39, 128.17, 127.68, 127.60, 127.51, 127.47, 126.53, 126.01, 125.80, 125.74, 125.20, 123.97, 122.66, 118.90, 15.46. MALDI– HRMS $(C_{98}H_{70}N_4Zn)^+$ Calcd: *m/z* = 1366.4892. Found: *m/z* = 1366.4879.

Synthesis of compound AN-BDP. Under nitrogen atmospher, triethylamine (4 mL) was added into the solution of compound 2 (65 mg, 0.1 mmol) and mixture was stirred at rt for 15 minutes. Afterwards, BF3Et2O (5 mL) was added dropwise into the above mixture at 0 ^{0}C and mixture was further stirred for two hours at rt. After completion of reaction, extracted with CH_2Cl_2 (30 mL), washed with water (2 × 100 mL) and dried over anhydrous sodium sulfate. After evaporation of solvent under reduced pressure, the crude product was further purified with column chromatography (Silica gel, CH_2Cl_2/petroleum ether, 1/3, v/v) to give blue solid (46 mg, yield: 65 %) NMR ($CDCl_3$, 400 MHz); δ ^{1}H NMR ($CDCl_3$, 400 MHz); δ 8.62 (s, 1H), 8.07 (d, 2H, *J* = 8.0 Hz), 8.02–7.98 (m, 6H), 7.95–7.84 (m, 8H), 7.54–7.43 (m, 10H) 6.64 (s, 2H), 0.75 (s,

6H). ^{13}C NMR (100 MHz, $CDCl_3$); δ152.92, 142.0, 141.93, 136.67, 134.24, 133.76, 133.60, 131.34, 130.14, 128.56, 128.44, 128.40, 128.34, 127.82, 127.07, 126.62, 126.51, 125.83, 125.27, 124.10, 119.57, 119.54, 117.96, 13.64. MALDI– MS ($[C_{49}H_{35}BF_2N_2]^+$) Calcd: *m/z* = 700.28. Found: *m/z* = 700.17.

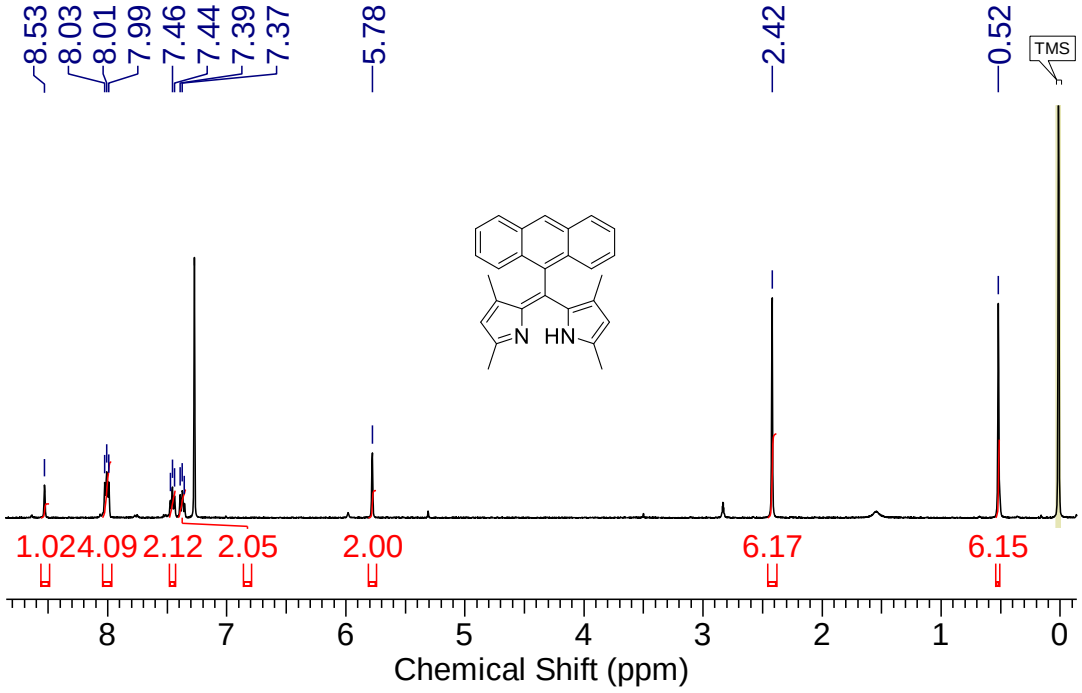

Figure S1. ^{1}H NMR of compound **1** (400 MHz, $CDCl_3$), 25°C

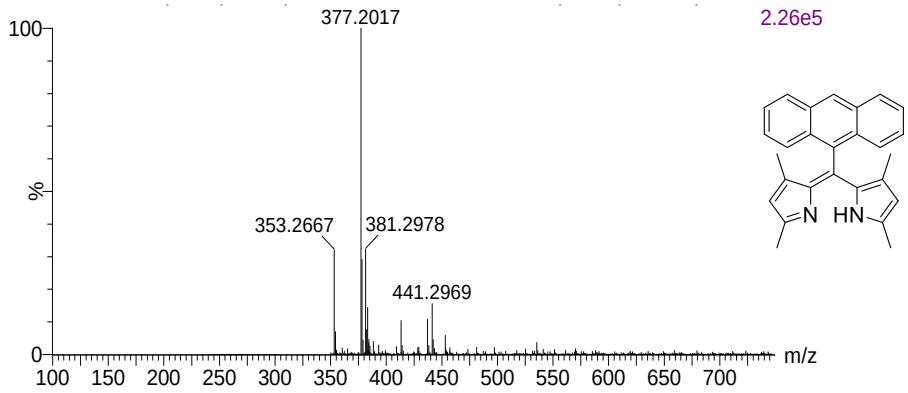

Figure S2. TOF ESI HR mass spectrum of compound **1**

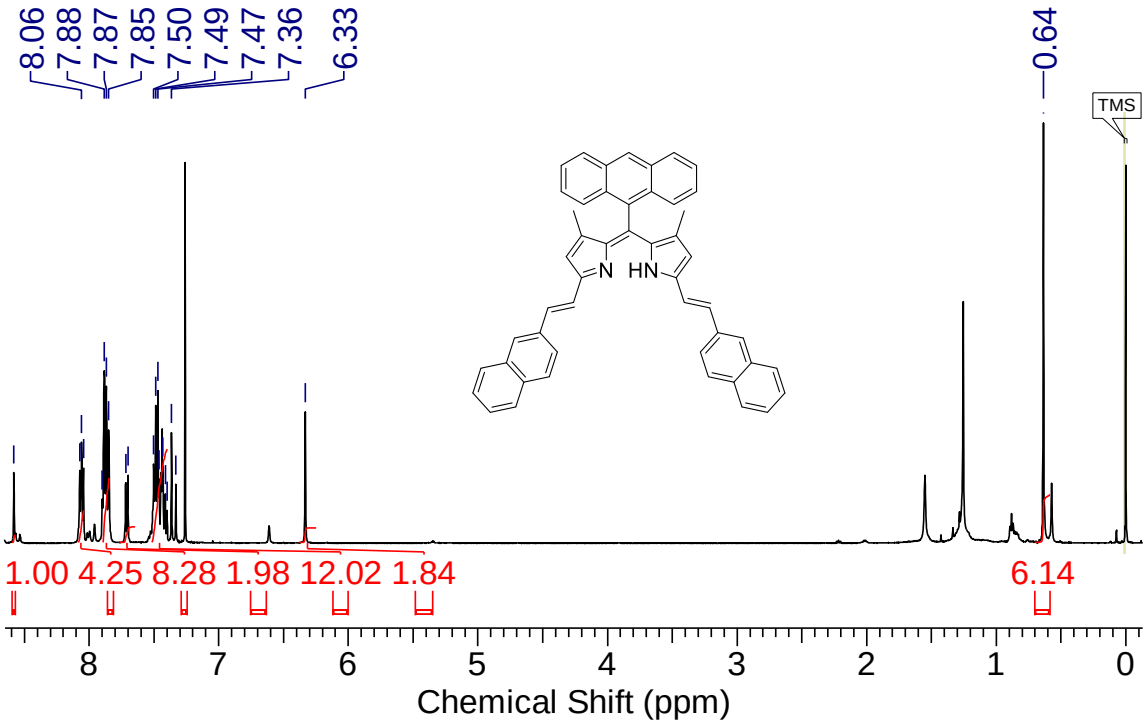

Figure S3. ^{1}H NMR of compound **2** (400 MHz, $CDCl_3$), 25°C

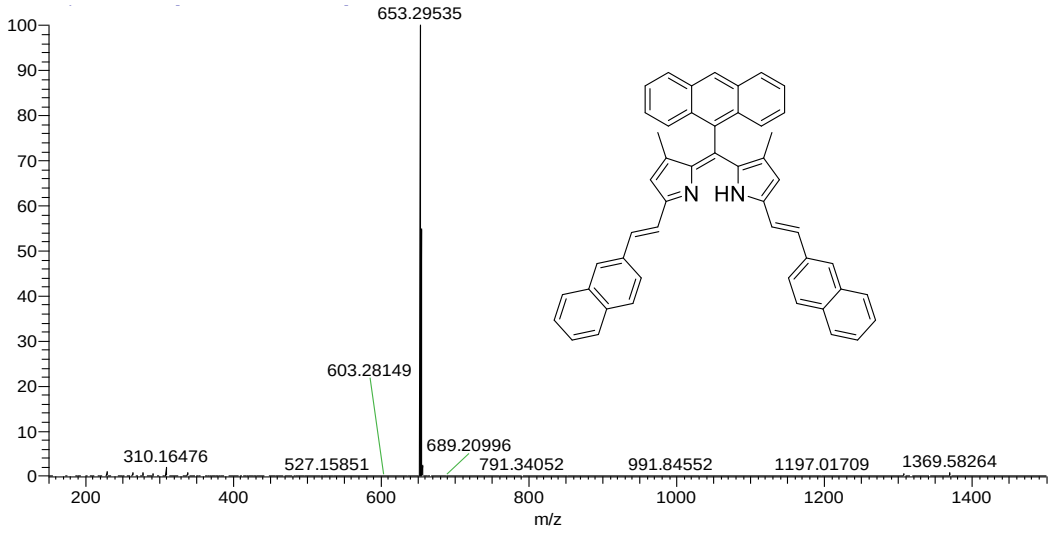

Figure S4. TOF ESI HR mass spectrum of compound **2**

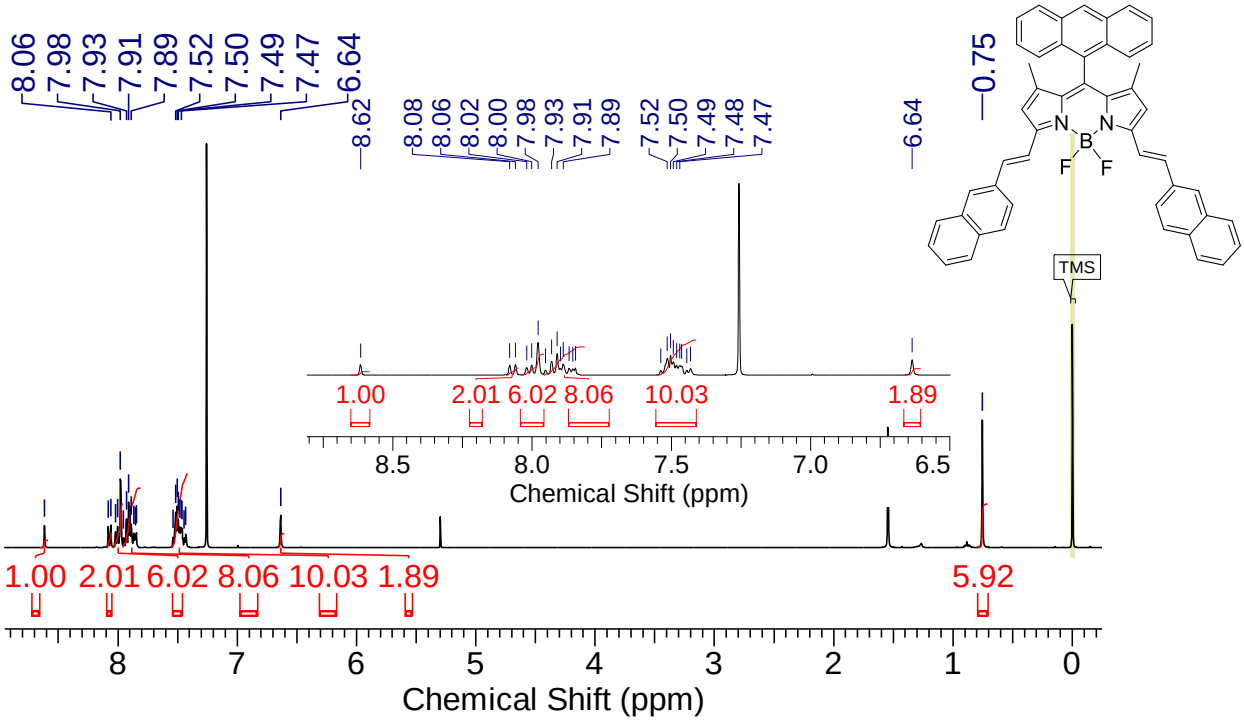

Figure S5. ^{1}H NMR of compound **AN-BDP** (400 MHz, $CDCl_3$), 25°C

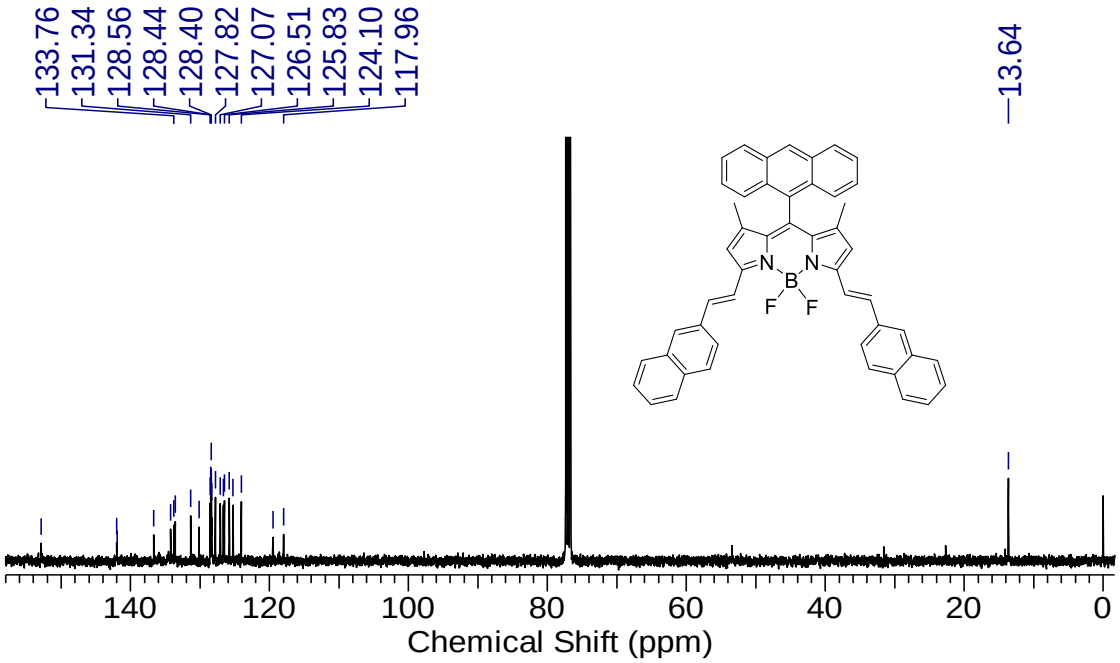

Figure S6. ^{13}C NMR of compound **AN-BDP** (100 MHz, $CDCl_3$), 25°C

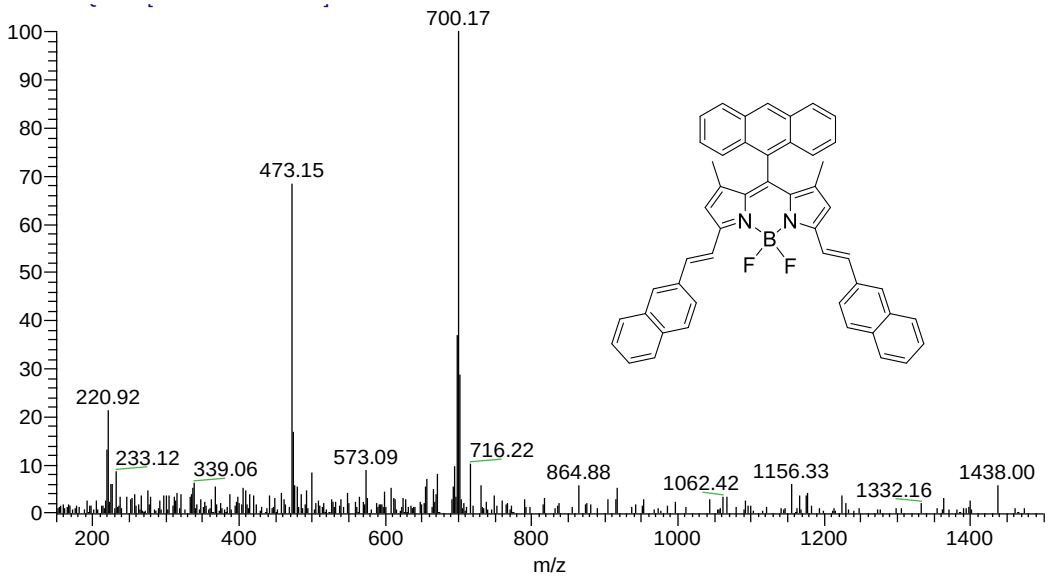

Figure S7. TOF ESI mass spectrum of compound **AN-BDP**

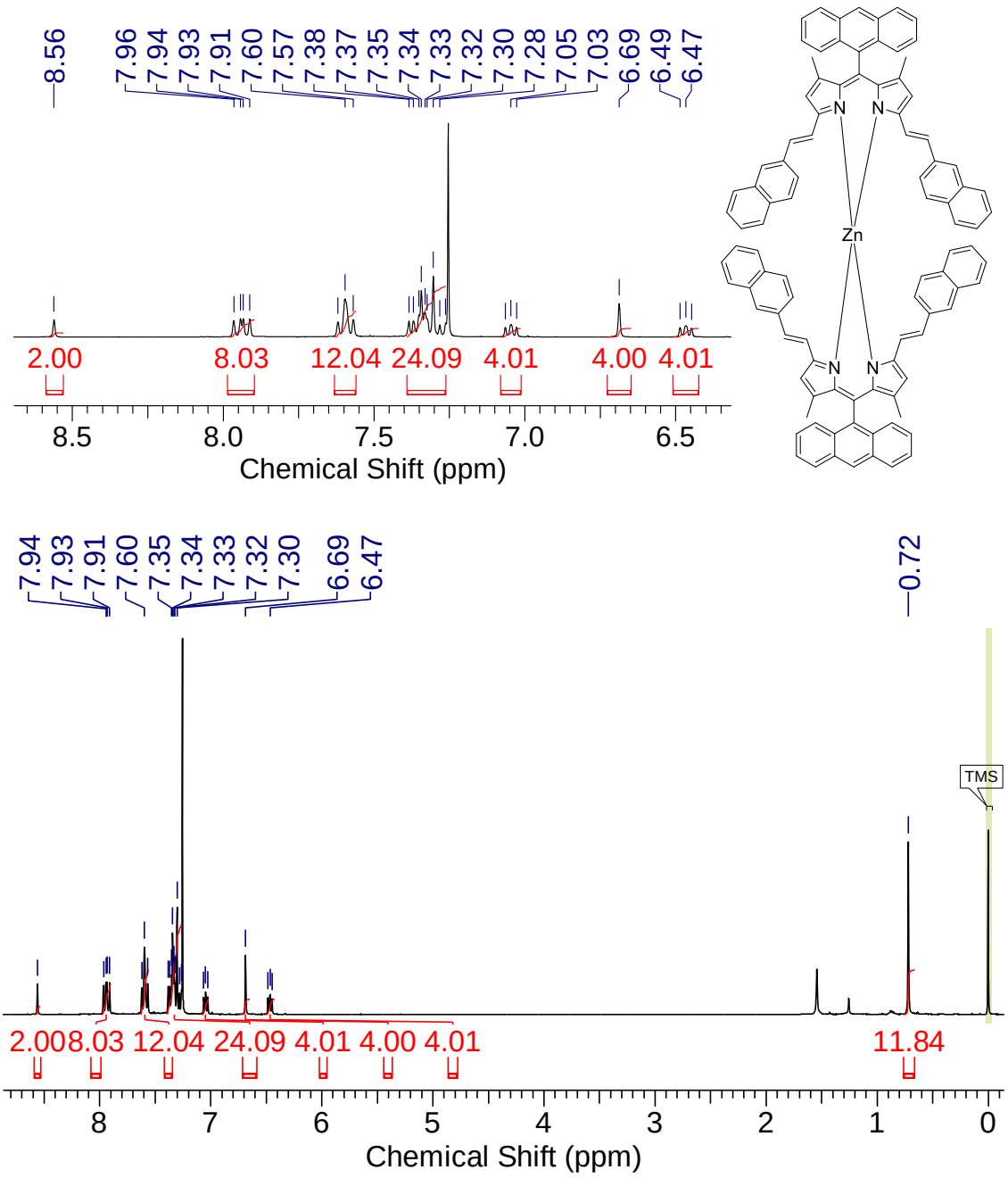

Figure S8. ^{1}H NMR of compound **AN-Zn** (400 MHz, $CDCl_3$), 25°C

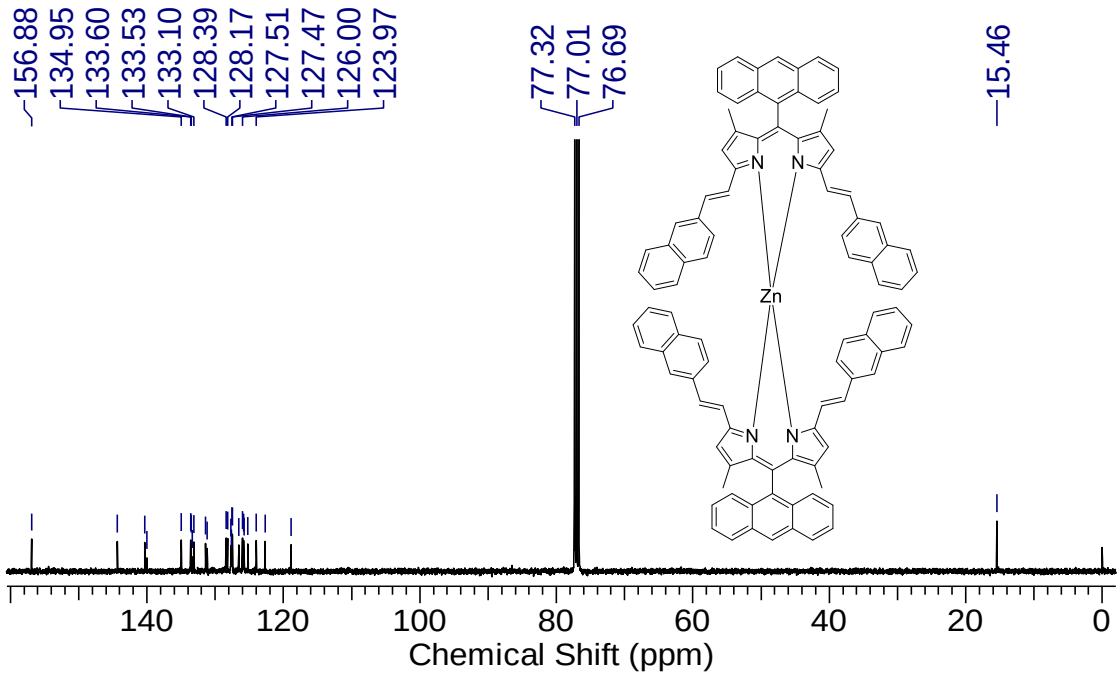

Figure S9. ^{13}C NMR of compound **AN-Zn** (100 MHz, $CDCl_3$), 25°C

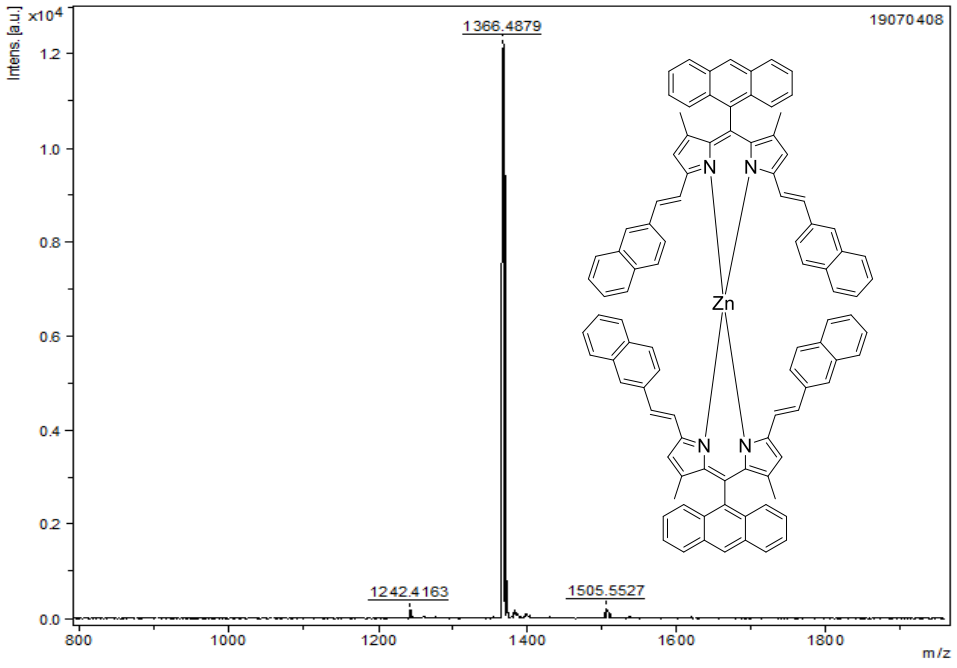

Figure S10. MALDI HR mass spectrum of compound **AN-Zn**

3. Photophysical Parameters of Compounds

Table S1. Photophysical parameters of bis(dipyrrin) complex and reference BDP derivatives.

		λ_{abs} [a]	ε [b]	λ_{em}	Φ_F [c]	τ_F [d] (ns)	Φ_Δ [e]
AN-ZN	HEX	623/368	14.8/9.7	658	0.10	3.2	0.10
	TOL	629/372	15.3/9.9	669	0.04	3.9	0.48
	DCM	628/372	15.3/9.9	667	0.005	4.0	0.80
	ACN	623/369	15.4/9.4	644	0.003	2.3	0.50
AN-BDP	HEX	640/367	8.7/4.8	653	0.53	4.2	–[f]
	TOL	652/371	8.3/4.3	667	0.47	4.8	–[f]
	DCM	647/370	7.9/4.4	664	0.47	4.1	–[f]
	ACN	641/370	7.8/4.5	657	0.45	4.2	–[f]
ST-BDP	HEX	618/344	11.3/9.6	625	0.75	4.9	–[f]
	TOL	628/350	11.1/8.1	638	0.59	4.6	–[f]
	DCM	623/348	9.9/7.8	634	0.68	4.9	–[f]
	ACN	616/343	10.3/8.0	626	0.69	5.0	–[f]

[a] In different solvents (1.0×10^{-5} M) and in nm. [b] Molar absorption Coefficient ($10^4\,M^{-1}cm^{-1}$). [c] Fluorescence quantum yield, Styryl-BDP was used as standard (Φ_F = 0.59 in toluene). [d] Luminescent lifetimes, λ_{ex} = 510 nm (laser). [e] Singlet oxygen quantum yield, methylene blue as stand (Φ_Δ = 0.57 in DCM). [f] Not applicable.

4. Theoretical Computations and Optimized Geometries

In order to elucidate the photophysical properties and get insight into electronic structure of zinc^{II} bis(dipyrrin) complexes and reference BDP derivative, density functional theory (DFT) computations were performed. The frontier molecular orbital supports the symmetry breaking charge transfer process in **AN-Zn**, as the HOMO is mainly confined on one dipyrrin unit while the LUMO is localized on both units. The degeneracy or negligible difference (0.02 eV) in the HOMO and HOMO−1 orbitals indicates no electronic coupling between the two dipyrrin units in complexes at the ground state. In case of **AN-BDP**, the HOMO and LUMO both are confined on the BDP moiety, indicating the negligible electronic communication among the BDP and anthracene unit, which is in accord with its high fluorescence quantum yield.

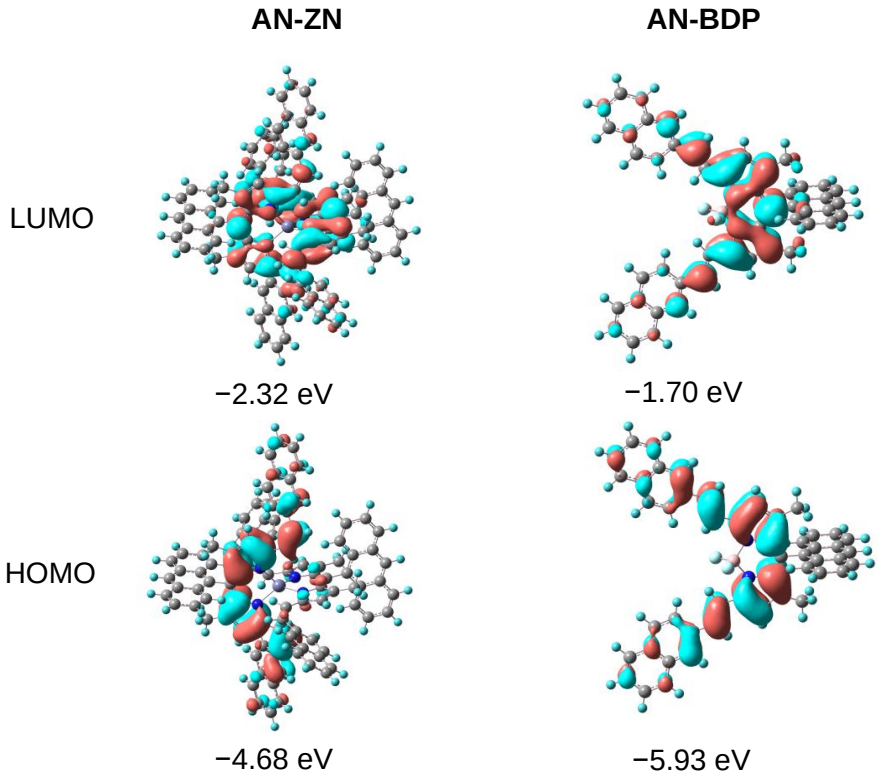

Figure S11. Frontier molecular orbitals (HOMO and LUMO) of bis(dipyrrin) complex **AN-Zn** and **AN-BDP** derivative calculated by DFT theory at (B3YLP/6-31G) level using Gaussian 09W.

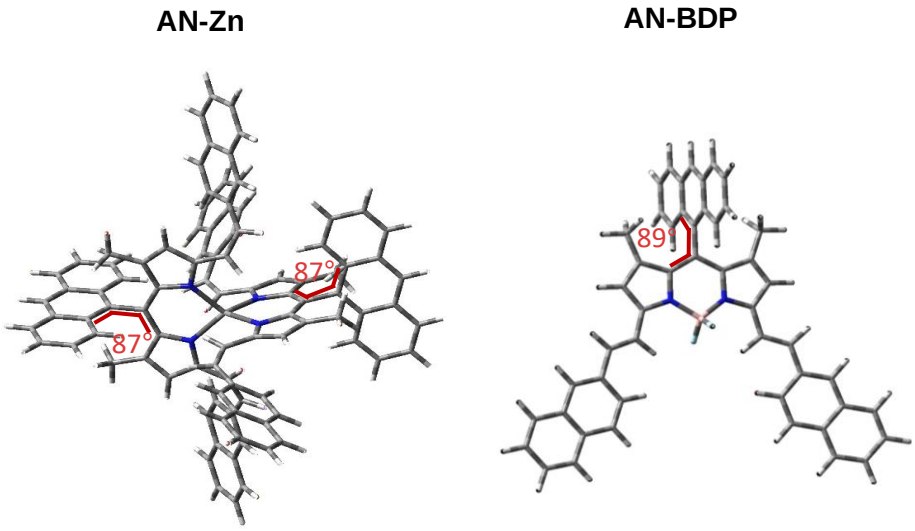

Figure S12. Optimized ground state geometry of bis(dipyrrin) complex **AN-Zn** and **AN-BDP** derivative calculated by DFT theory at (B3YLP/6-31G) level using Gaussian 09W.

The spin density of triplet state (T_1) was also computed using the DFT and interestingly it was observed that the electron density is confined on the styryl dipyrrin unit, in line with nanosecond transient absorption study, showing the population of typical styryl dipyrrin triplet state. No spin density was observed on the Zinc atom, which excluded its role in the population of triplet state. Moreover, the confinement of triplet spin density on one dipyrrin unit also support the excited state symmetry breaking process in the bis(dipyrrin) complex.

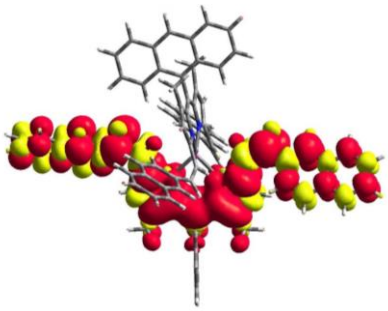

Figure S13 Spin density distribution of the triplet states of **An-Zn** obtained by computation with DFT theory at (B3YLP/6-31G/LANL2DZ) level using Gaussian 09W.

5. UV/Vis absorption spectra

Solvent-dependency UV Vis absorption of compounds

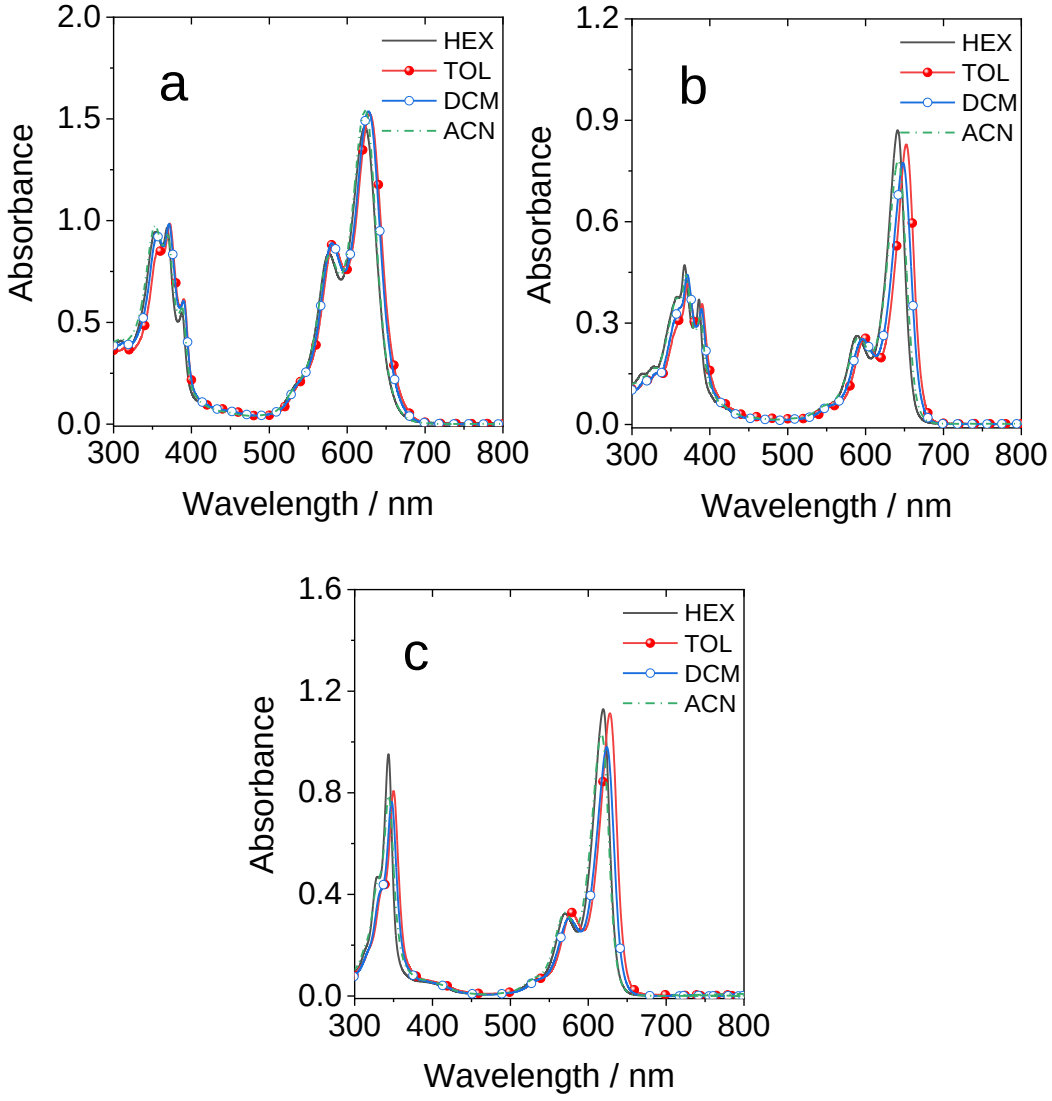

Figure S14. UV/Vis absorption spectra in different solvents of (a) **AN-Zn**; (b) **AN-BDP**; and (c) **ST-BDP**. $c = 1.0 \times 10^{-5}$ M; 20 ^{0}C.

6. Fluorescence emission spectra

Solvent-dependent fluorescence emission of compounds

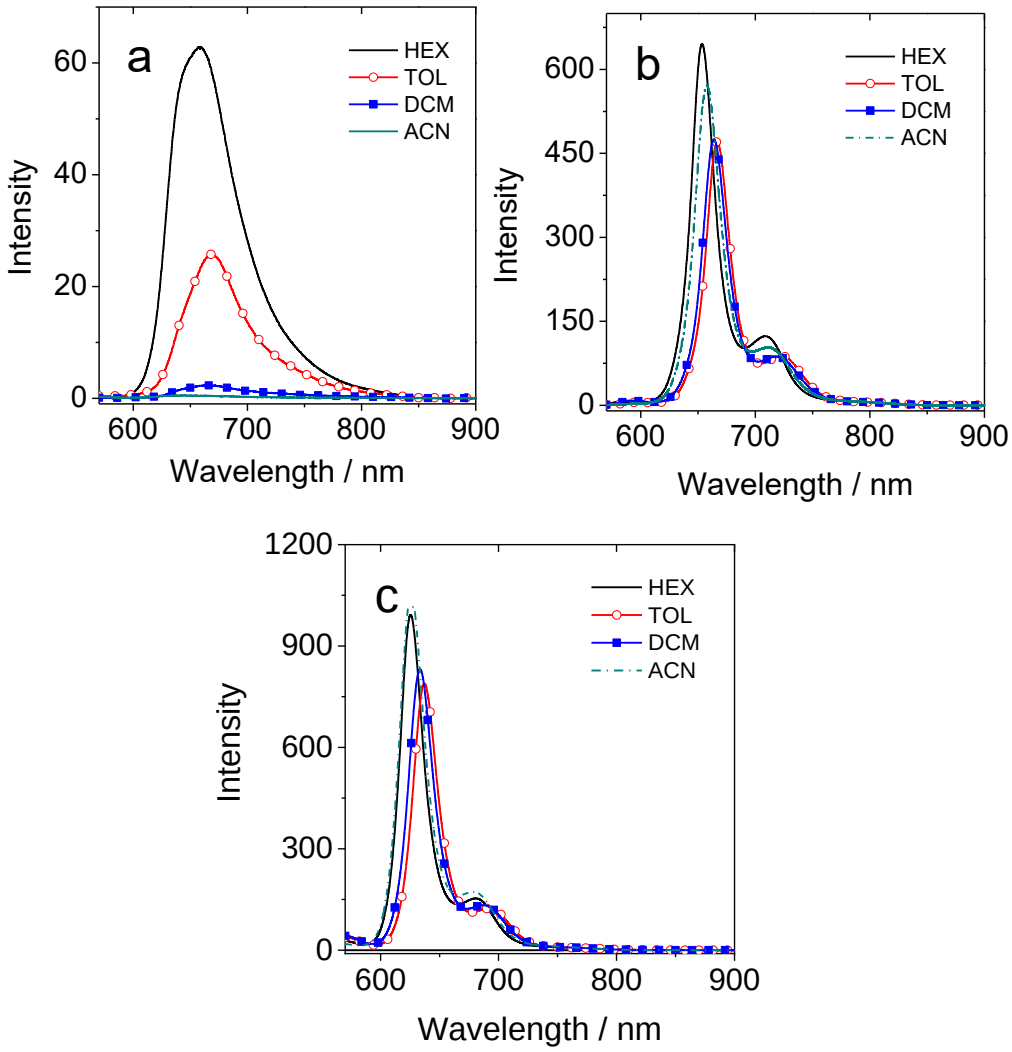

Figure S15. Fluorescence emission spectra of compounds; (a) **AN-Zn**; (b) **AN-BDP**; and (c) **ST-BDP**. λ_{ex} = 565 nm (A = 0.10). Optically matched solution were used (All the compounds have same absorbance at the excitation wavelength); 20 ^{0}C.

7. Fluorescence emission decay curves

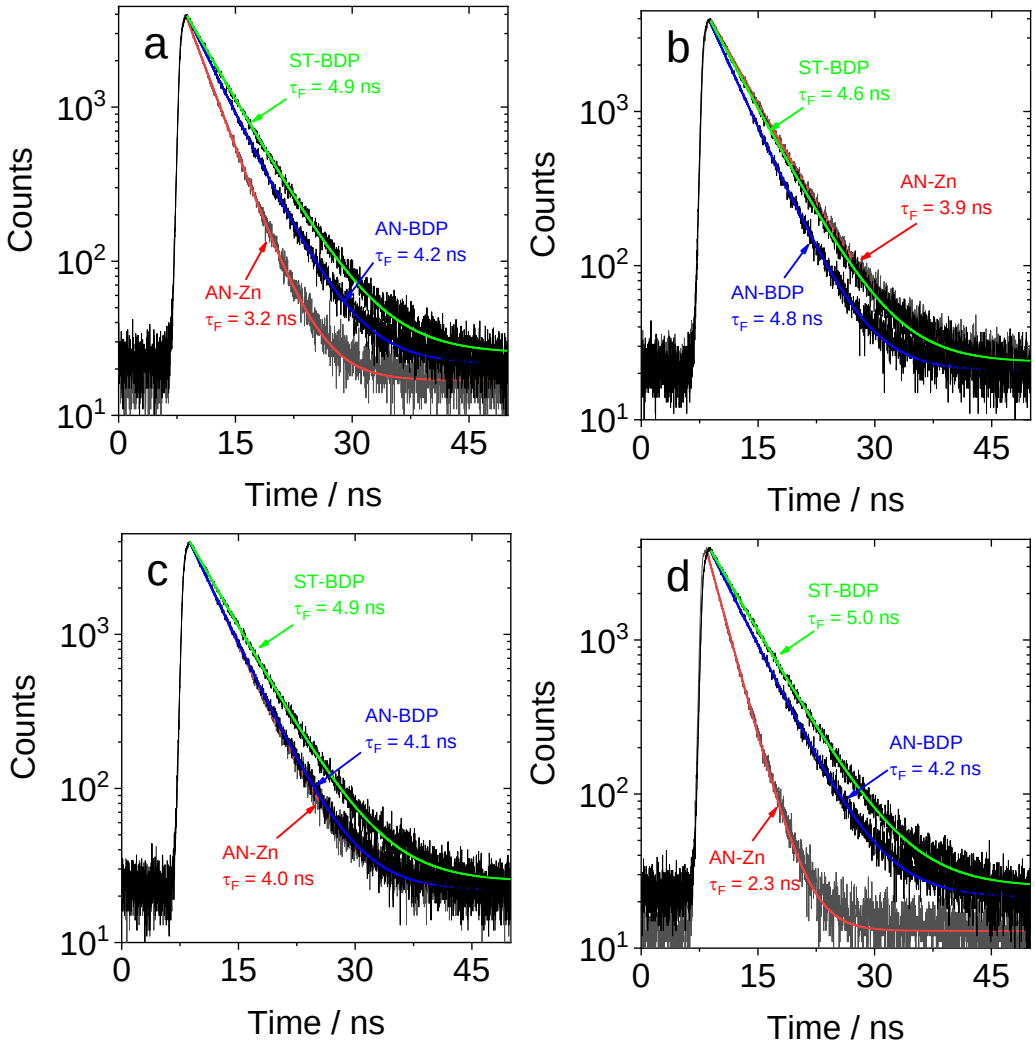

Figure S16. Fluorescence emission decay traces of bis(dipyrrin) complex along with their reference compounds in (a) *n*-hexane; (b) toluene; (c) dichloromethane; and (d) acetonitrile, (λ_{ex} = 510 nm), monitored at 665 nm for **AN-Zn**; 655 nm for **AN-BDP** and 650 nm for **ST-BDP**, respectively. $c = 1.0 \times 10^{-5}$ M, 20 °C.

8. Fluorescence Excitation Spectra

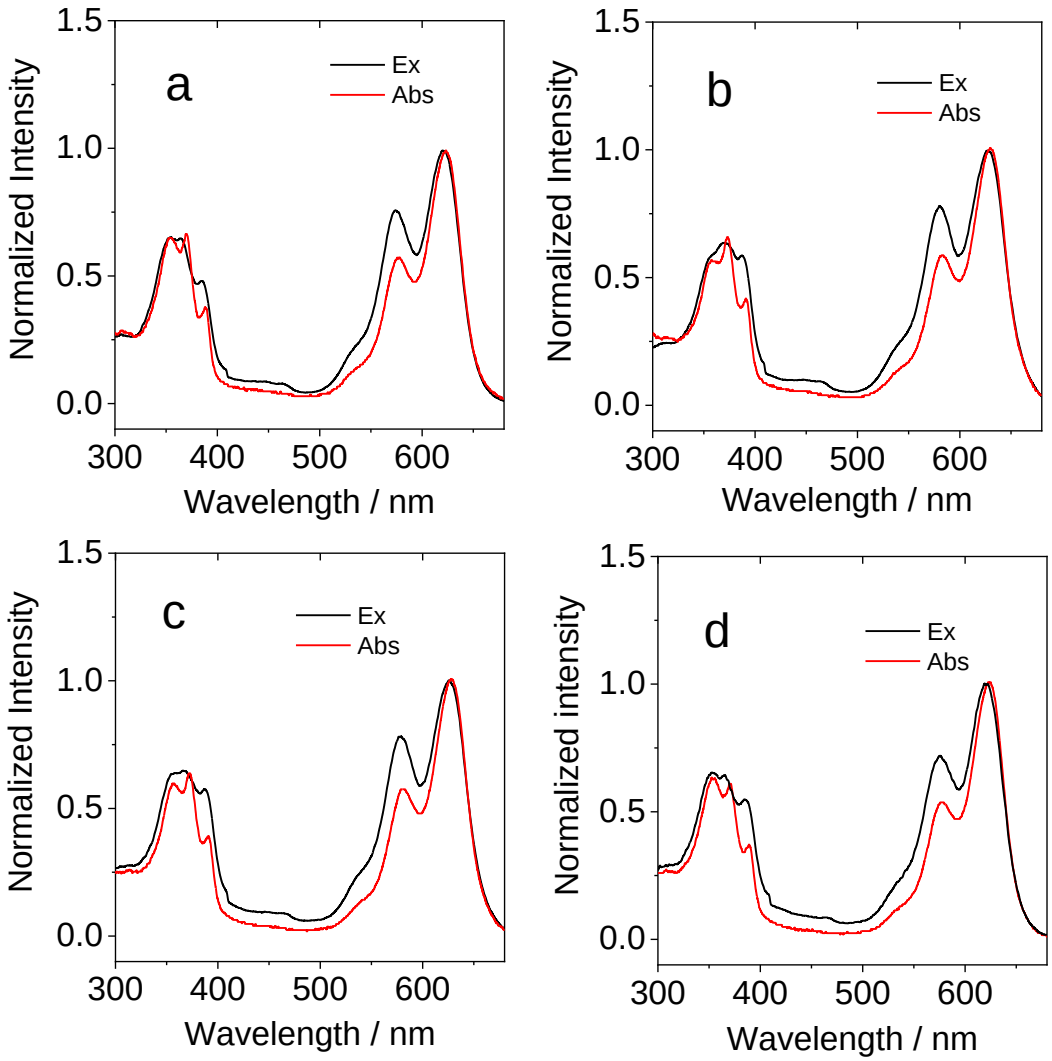

Figure S17. Comparison of Normalized UV-Vis absorption and the excitation dependent photoluminescence spectra of **AN-Zn** in (a) *n*-hexane; (b) toluene; (c) dichloromethane; and (d) acetonitrile, (λ_{em} = 710 nm); 20 ^{0}C.

For further insight in the photophysical process involved in **AN-Zn** and reveal the origin of fluorescence, the excitation dependent luminescence spectra of **AN-Zn** in the range of 300-700 nm in different solvent were obtained (Fig. S17). Measurement of excitation dependent luminescence is considered a most useful and effective tool to confirm the origin of emission. The obtained excitation spectra were normalized with absorption and comparison shows that, there is no distinct change in the peaks, thus confirm that the emission originate from the **AN-Zn**. However, a slight change in the intensity was observed. Briefly, the observed fluorescence excitation spectra is not a superimposed image of absorption spectra, instead higher excitation energy was observed at one high energy vibronic shoulder absorption band. This indicates the excited state vibronic interaction among the two dipyrrin units due to presence of different extent of coupling among the two unit at the ground and excited state. The obtained results are also similar with reported excitation dependent photoluminescence study of bis(dipyrrin) complexes.[6] Further advance studies, such as excitation dependent emission and transient absorption needed to confirm the above postulate which is out of the scope of the paper and will conduct a separate in-depth study in the near future.

9. Redox properties of compounds.

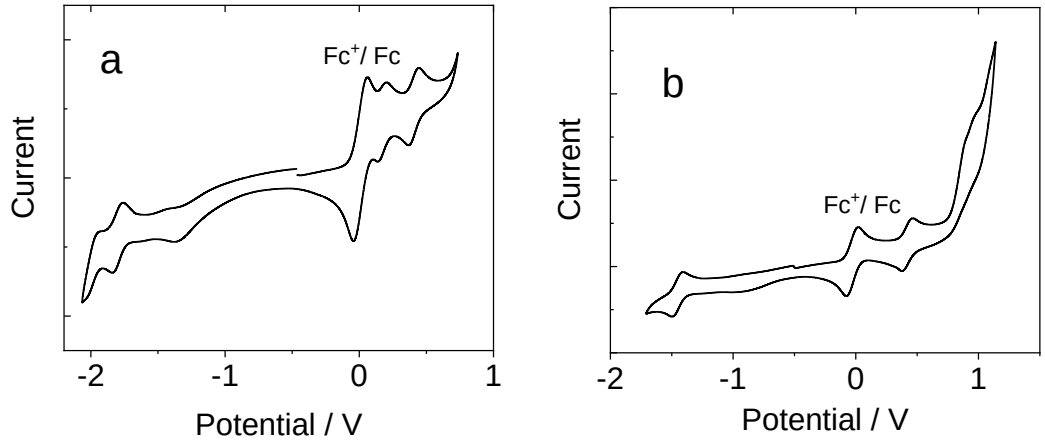

Figure S18. Cyclic voltammogram of compounds, (a) **AN-Zn**; and (b) **AN-BDP** in deaerated dichloromethane, containing 0.10 M Bu_4NPF_6 as supporting electrolyte, Ferrocene (Fc) was used as the internal reference. Scan rates: 50 mV/s. $c = 5 \times 10^{-4}$ M, 20 °C.

For **AN-BDP,** one reversible reduction wave at – 1.45 V and one reversible oxidation wave at +0.42 V were recorded, which can be assigned to Styryl BDP moiety. One irreversible oxidation wave at +0.98 V, belonging to anthracene unit, was also observed. The cyclic voltammogram of **AN-Zn**, showed one reversible reduction wave at – 1.79 V and two reversible oxidation waves at +0.18 V and +0.40 V, respectively, assigned to Styryl dipyrrin moiety.

The thermodynamical feasibility for excited state SBCT in **AN-Zn** and PET among anthracene and styryl BDP acceptor in **AN-BDP** are calculated employing Rehm−Weller analysis.

$$\Delta G^0{}_{\mathrm{CS}} = e[E_{OX} - E_{RED}] - E_{00} + \Delta G_{\mathrm{S}} \qquad \text{(Eq. 2)}$$

$$\Delta G_{\mathrm{S}} = -\frac{e^2}{4\pi\varepsilon_{\mathrm{S}}\varepsilon_0 R_{\mathrm{CC}}} - \frac{e^2}{8\pi\varepsilon_0}\left(\frac{1}{R_D} + \frac{1}{R_{\mathrm{A}}}\right)\left(\frac{1}{\varepsilon_{REF}} - \frac{1}{\varepsilon_S}\right) \qquad \text{(Eq.3)}$$

Where ΔG_S is the static Coulombic energy, which is described by eq. 3. e = electronic charge, E_{OX} = half-wave potential for one-electron oxidation of the electron-donor unit, E_{RED} = half-wave potential for one-electron reduction of the electron-acceptor unit; E_{00} = energy level approximated with the fluorescence emission (for the singlet excited state), ε_S = static dielectric constant of the solvent, R_{CC} = center-to-center separation distance between the electron donor (carbazole) and electron acceptor (BDP), determined by DFT optimization of the geometry, R_D is the radius of the electron donor, R_A is the radius of the electron acceptor, ε_{REF} is the static dielectric constant of the solvent used for the electrochemical studies, ε_0 is permittivity of free space. The solvents used in the calculation of free energy of the electron transfer are toluene (ε_S = 2.38), CH_2Cl_2 (ε_S = 8.93) and acetonitrile (ε_S = 37.5).

$$E_{CS} = e[E_{OX} - E_{RED}] + \Delta G_S \qquad \text{(Eq. 4)}$$

$$\Delta G_{CR} = -(\Delta G_{CS} + E_{00}) \qquad \text{(Eq. 5)}$$

Table S2. Driving Forces of Charge Recombination (ΔG^0_{CR}) and Charge Separation (ΔG^0_{CS}) and the Energy of Charge Separated State (CSS) for compounds [a]

	ΔG^0_{CS} (eV)			ΔG^0_{CR} (eV)			E_{CSS} (eV)		
	TOL	DCM	ACN	TOL	DCM	ACN	TOL	DCM	CAN
AN-Zn [a]	–0.08	–0.24	–0.29	–1.86	–1.69	–1.64	1.86	1.69	1.64
AN-BDP [b]	0.22	0.18	0.17	–2.11	–2.08	–2.07	2.11	2.08	2.07

[a] E_{00} = 1.93 eV, [b] E_{00} = 1.89 eV. E_{00} is the approximated energy level with the cross point of UV−Vis absorption and fluorescence emission after normalization at the singlet excited state.

10. Nanosecond Time-resolved Difference Absorption Spectra

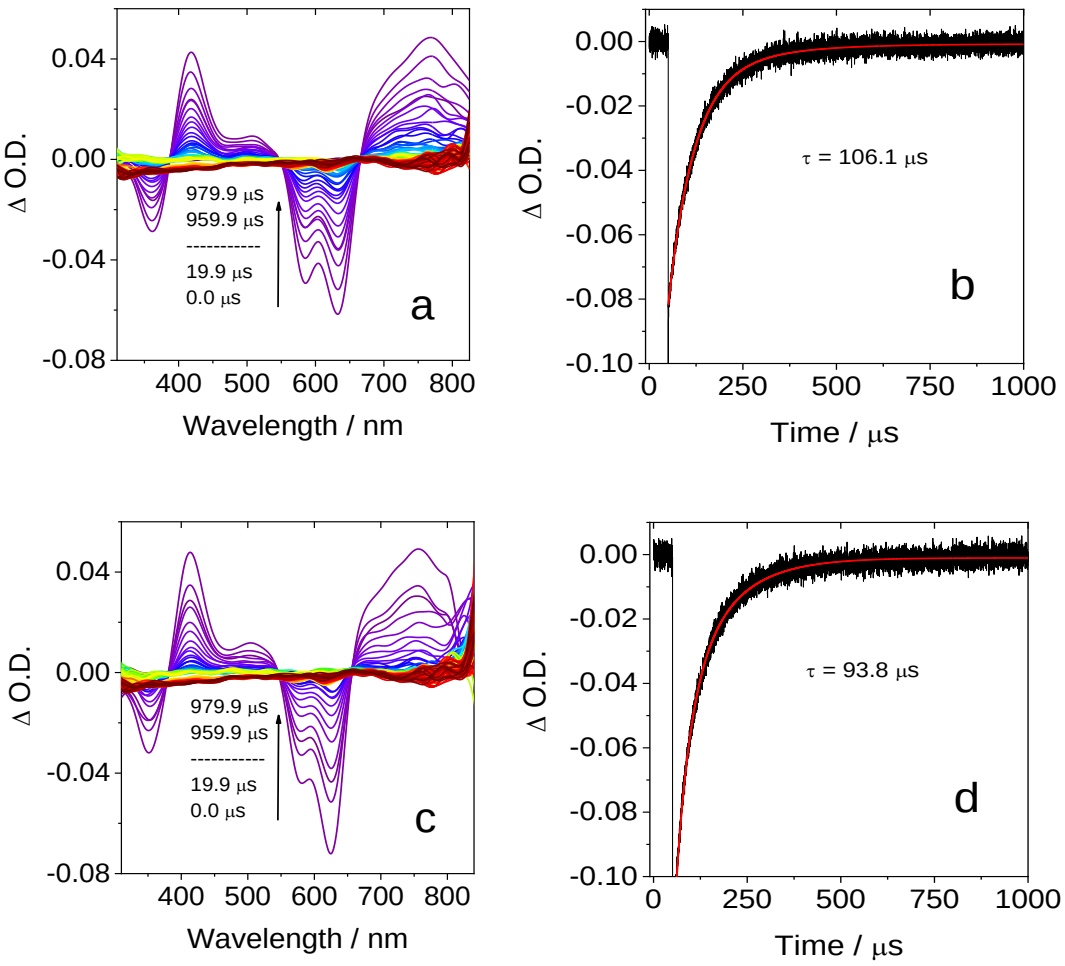

Figure S19. Nanosecond transient absorption spectra of **AN-Zn**; (a) in deaerated toluene and (c) in acetonitrile, upon ns pulsed laser excitation (λ_{ex} = 600 nm). Fig (b) and (d) are their respective decay curves at 630 nm, $c = 5.0 \times 10^{-6}$ M, 20 °C.

11. Femtosecond Transient Absorption Spectra

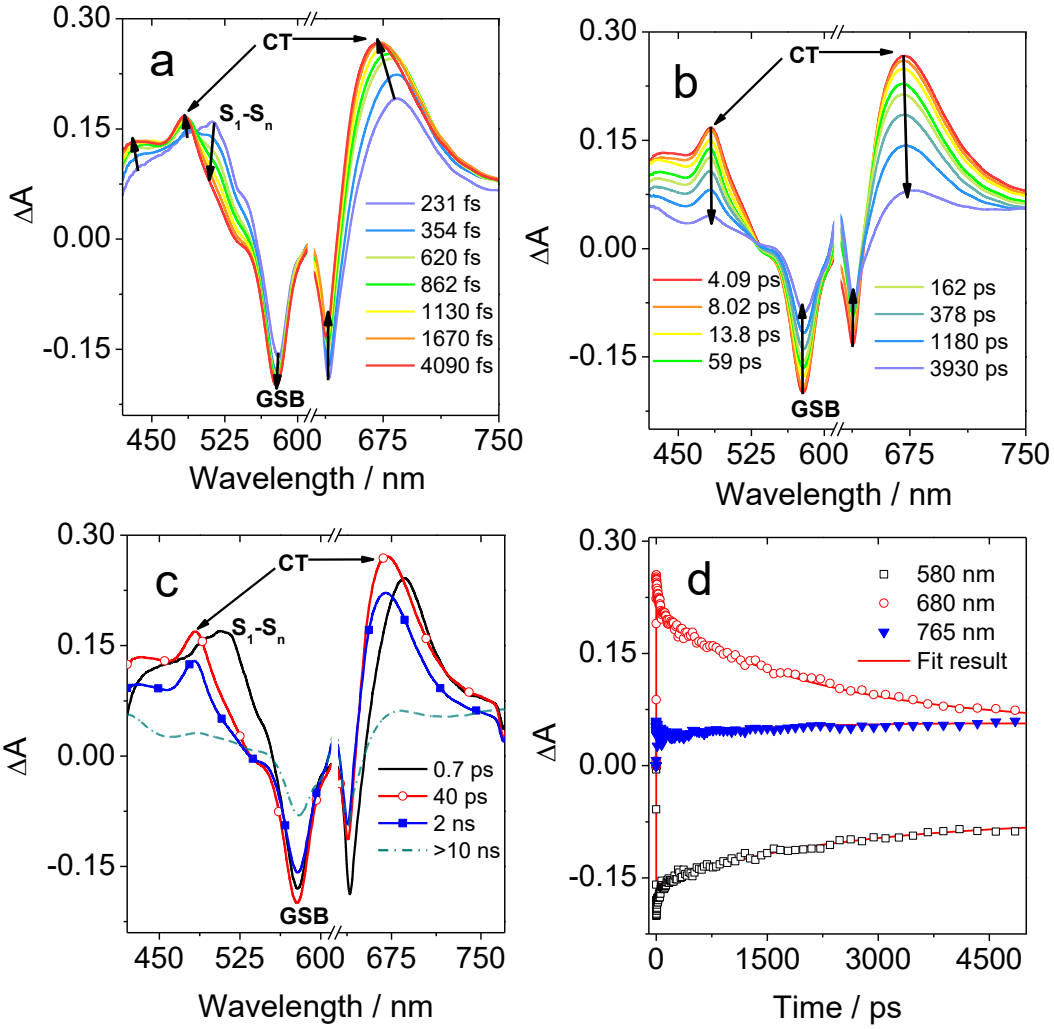

Figure S20. (a) Femtosecond transient absorption spectra of **AN-Zn** in dichloromethane at short time delay, (b) at long time delay. (c) Evolution associated difference spectra (EADS) and (d) Decay trace at selected wavelength. λ_{ex} = 625 nm, c=1×10^{-5} M, 20 °C.

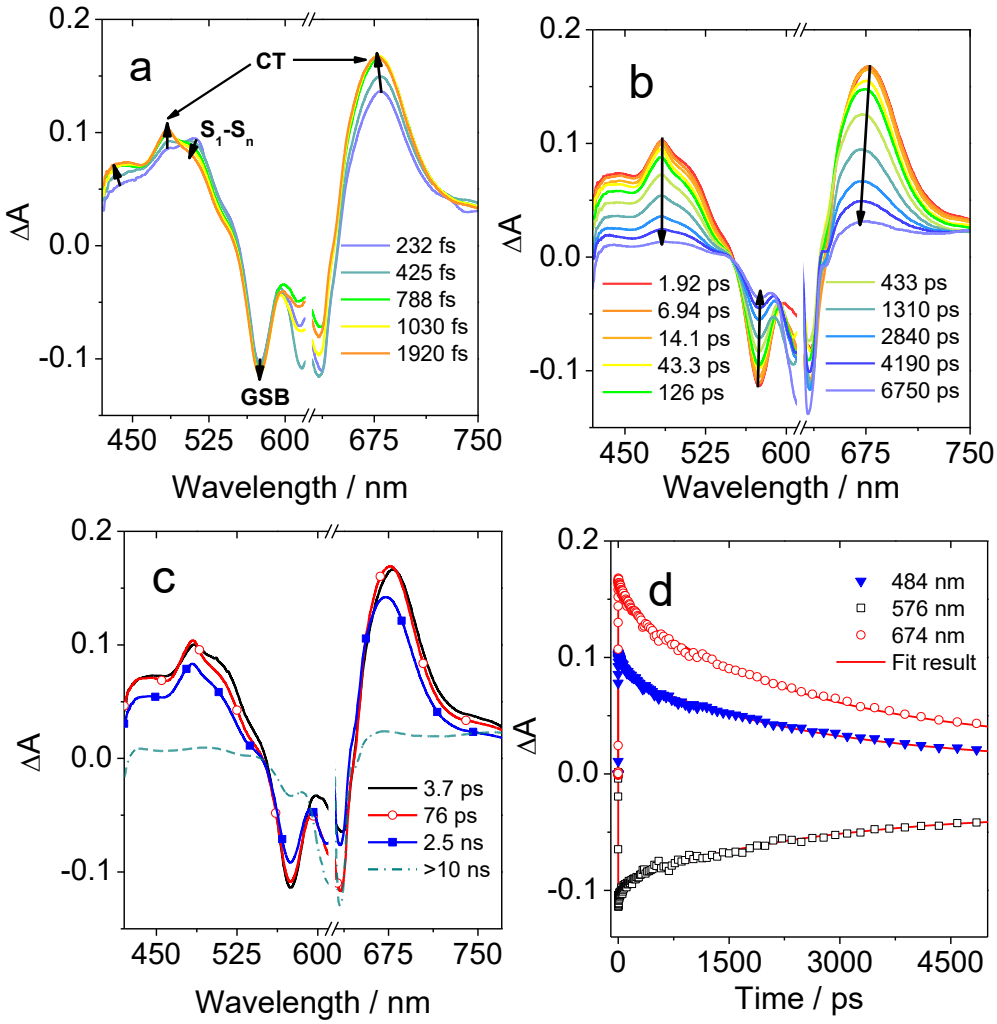

Figure S21. (a) Femtosecond transient absorption spectra of **AN-Zn** in *n*-hexane at short time delay, (b) at long time delay. (c) Evolution associated difference spectra (EADS) and (d) Decay trace at selected wavelength. λ_{ex} = 625 nm, c=1×10^{-5} M, 20 °C.

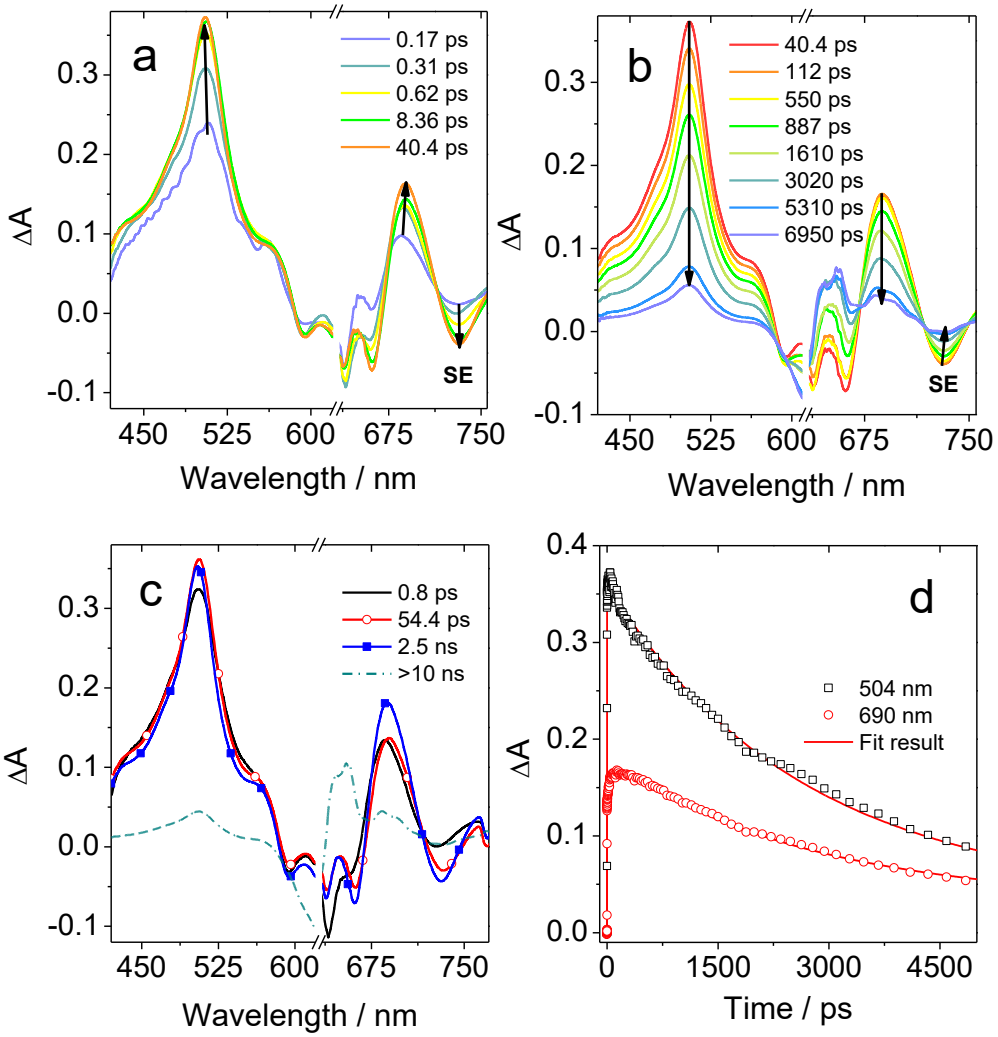

Figure S22. (a) Femtosecond transient absorption spectra of **AN-BDP** in dichloromethane at short time delay, (b) at long time delay. (c) Evolution associated difference spectra (EADS) and (d) Decay trace at selected wavelength. λ_{ex} = 625 nm, c=1×10^{-5} M, 20 °C.

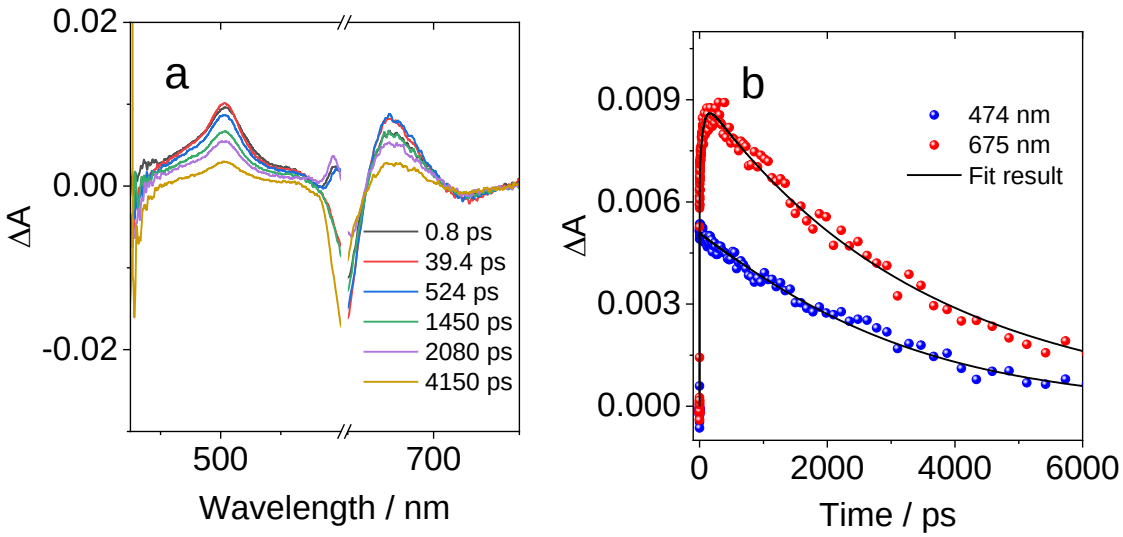

Figure S23. (a) Femtosecond transient absorption spectra of **AN-BDP** in hexane at different time delay, and (d) Decay trace at selected wavelength. λ_{ex} = 625 nm, c=1×10^{-5} M, 20 °C.

12. Photophysical process and Jablonski Diagram

The overall photophysical process involved in **AN-Zn** can be depicted by the following Jablonski diagram. Upon photoexcitation, the excited state symmetry breaks and charge transfer takes place from one dipyrrin unit to another dipyrrin unit and afterwards the triplet state populates via charge recombination following the spin-orbit charge transfer intersystem crossing (SOCT-ISC) mechanism.

Scheme 2: Jablonski Diagram Demonstrating the Photophysical Processes Involved in AN-Zn upon Photoexcitation [a]

AN-Zn compound is a symmetric bichromophoric system and consist of two identical styryl dipyrrin units connecting each other through zinc bridge and don't exhibit any electronic communication due to similar redox potential. However, symmetry breaking at the excited state is responsible for charge transfer from one unit to the other, which leads to population of charge separated state. Later, triplet state of bis(dipyrrin) populates via charge recombination.

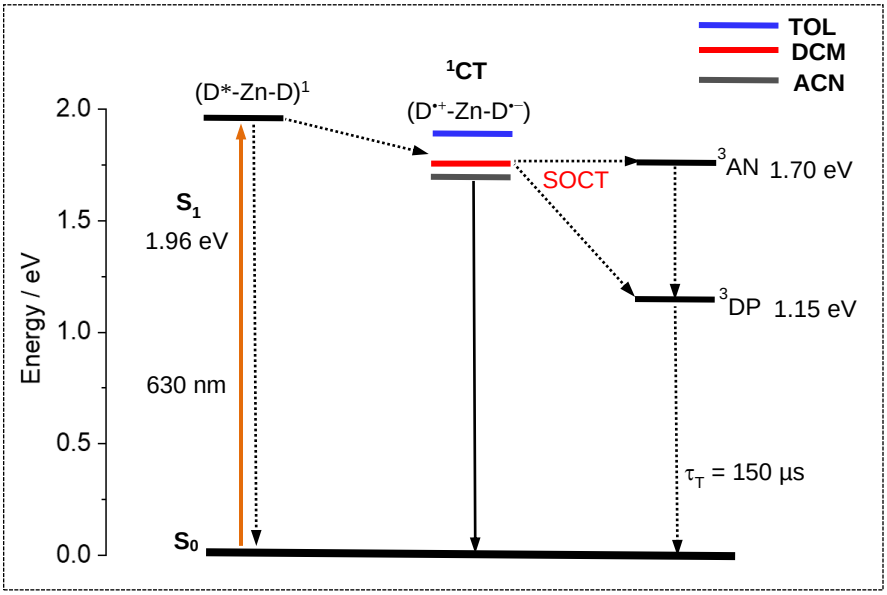

a The energy levels of the excited singlet states are derived from the spectroscopic data; the energy level of charge transfer state are obtained from electrochemical data. The triplet energy levels are estimated by TD-DFT method. The numbers in the superscripts indicates the spin multiplicity, D and DP indicates the styryl dipyrrin unit while AN stands for anthracene moiety.

13. Photopolymerization of methyl methacrylate

General Polymerization Procedure: A 3 mL vial was charged with a small stir bar, methyl methacrylate (4.67 mmol, 0.5 mL), ethylene glycol dimethacrylate (0.23 mmol, 44 μL), methyl α-bromophenylacetate (0.635 mmol, 100 μL), **AN-Zn** (0.4 mg, 0.0125 mol%) photosensitizer, perylenebisimide (PBI, 0.6 mg, 0.025 mol%) acceptor and triethylamine (8.1 μL, 1.25 mol%) sacrificial reagent under the nitrogen atmosphere. Afterwards, the vial was sealed and transferred to red-light source under the shield of aluminum foil. The reaction vessel was then irradiated with 620 nm red LED (power density: 60-70 mW/cm^{-2}) for 1 hour 30 minutes, to obtain the standing gel. Various controlled experiments were performed. Firstly, the reaction works only under deaerated conditions and quenched by presence of oxygen. Second, without **AN-Zn** and PBI, the polymerization of MMA didn't work, confirming the involvement of both **AN-Zn** and PBI in the polymerization process. Then we performed the polymerization experiment using the standard conditions but with the addition of the electron capturing reagent TEMPO and found that reaction ceased. This indicates the involvement of free radical in the polymerization process, which is also in line with previous reports.[7]

To clarify the mechanism, we performed the steady state and transient absorption study of **AN-Zn**, in the presence of PBI upon red light illumination. Firstly, the absorption of **AN-Zn** was recorded which showed an intense absorption band at 630 nm. Then the absorption of mixture **AN-ZN**, and PBI was measured which showed the two characteristic absorption bands at 630 and 522 nm, associated with **AN-Zn** and PBI respectively. Upon photoirradiating the mixture with red light (620 nm laser), the PBI absorption at 522 nm decreased, and new NIR absorption bands at 701, 798 and 995 nm appeared and intensified with irradiating time, which are the

characteristic $D_0 \rightarrow D_n$ absorption of $PBI^{\bullet -}$.[8] From this study, we suppose the electron transfer takes place from triplet state of **AN-Zn** to PBI moiety, because no radical formation was observed in air. We also revised the experiment in the presence of sacrificial reagent triethylamine (TEA) and more pronounced changes was observed, indicating the quantum yield of $PBI^{\bullet -}$ formation increases. This is reasonable because we also expect the triplet energy transfer from **AN-Zn** to PBI, which populates the triplet state of PBI moiety, followed by the generation of $PBI^{\bullet -}$ in the presence of sacrificial reagent. This assumption was confirmed by the controlled experiment and nanosecond transient absorption study. Moreover, upon exposure the mixture on air, the NIR absorption band associated with $PBI^{\bullet -}$ disappeared and PBI absorption restored, which further confirmed the formed species are $PBI^{\bullet -}$ that oxidized to neutral species in air. This phenomenon is repeatable upto many cycles. Further, the controlled experiment revealed that on photoexciting only PBI solution in presence of TEA, under the same experimental condition, no $PBI^{\bullet -}$ formation was observed as PBI lacks ISC. The nanosecond transient absorption study confirmed the triplet-triplet energy transfer from **AN-Zn** to PBI moiety as evidenced by population of the PBI triplet state and significant reduction in **AN-Zn** triplet lifetime. Thus, from these results we suppose following is the overall mechanism of the MMA polymerization. Based on the spectroscopic measurements, controlled experiments and previous reports, we assumed that there are two plausible pathways for the formation PBI radical anion in our system, i.e., photoinduced electron transfer or triplet-triplet energy transfer (TTET) from **AN-Zn** to PBI. Simply, upon photoexcitation of resin with red light, exciting the **AN-Zn** compound and its triplet state is populated which either reductively quenched via photoinduced electron transfer to PBI generating $PBI^{\bullet -}$ or decay via TTET to the PBI moiety populating the PBI triplet state. The populated $^3PBI^*$ may also reduce in presence of sacrificial reagent TEA and

finally generates the $PBI^{\bullet-}$, which undergoes excitation and initiate the MMA polymerization following the protocol as previously reported.[7] Briefly, TTET and PET processes may compete with each other, however TTET is found to be a dominant channel in the current conditions.

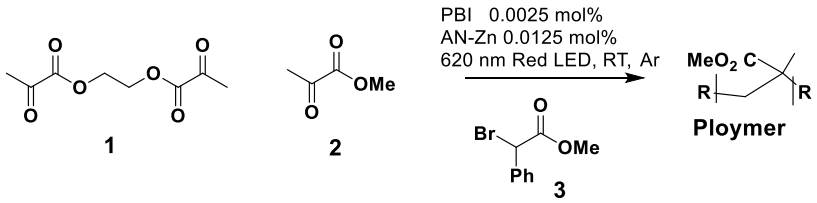

Optimized conditions of the photopolymerization: Red LED (60-70 mW/cm^{-2})

Compound 1: Ethylene Glycol Dimethacrylate (Crosslinker additive) = 0.235mmol (44uL)

Compound 2: Methyl Methacrylate (Monomer) = 4.675mmol (0.5mL)

Compound 3: Methyl α-Bromophenylacetate = 0.635mmol (100uL)

Catalysts loading:

AN-ZN = (0.0125mol%) 0.4mg & **PBI** (0.025mol%) 0.6mg

Sacrificial reagent:

Triethylamine (TEA) = (1.25mol%) 8.1uL

	PBI+TEA	AN-Zn	Light	Time	State
1	0.025mol% + 1.25mol%	-	Red LED	1.5 h	×
2	-	0.025mol%	Red LED	1.5 h	×
3	0.025mol% + 1.25mol%	0.025mol%	Red LED	1.5 h	Gel

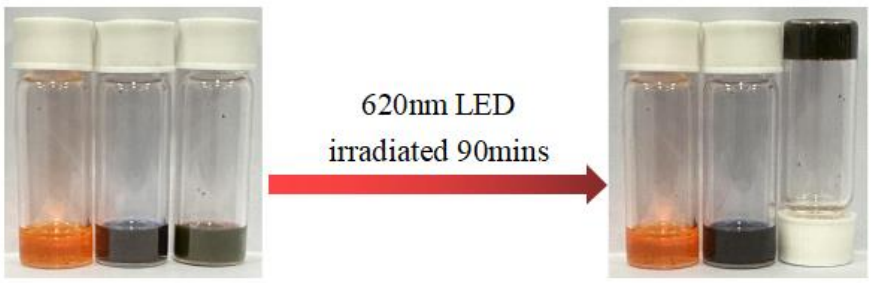

Before irradiation **After irradiation**

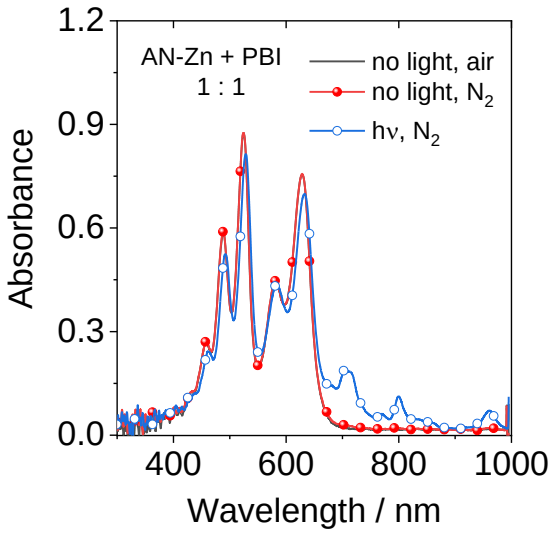

Figure S24. UV-Vis absorption spectra of **AN-Zn** in the presence of PBI in the deaerated dimethylformamide upon photoirradiation with red light (power density: 60-70 mW/cm^{-2}) for 5 minutes, *c* (**AN-Zn)** = 5×10^{-6} M and *c* (**AN-Zn)** = 1×10^{-5} M, 20 °C.

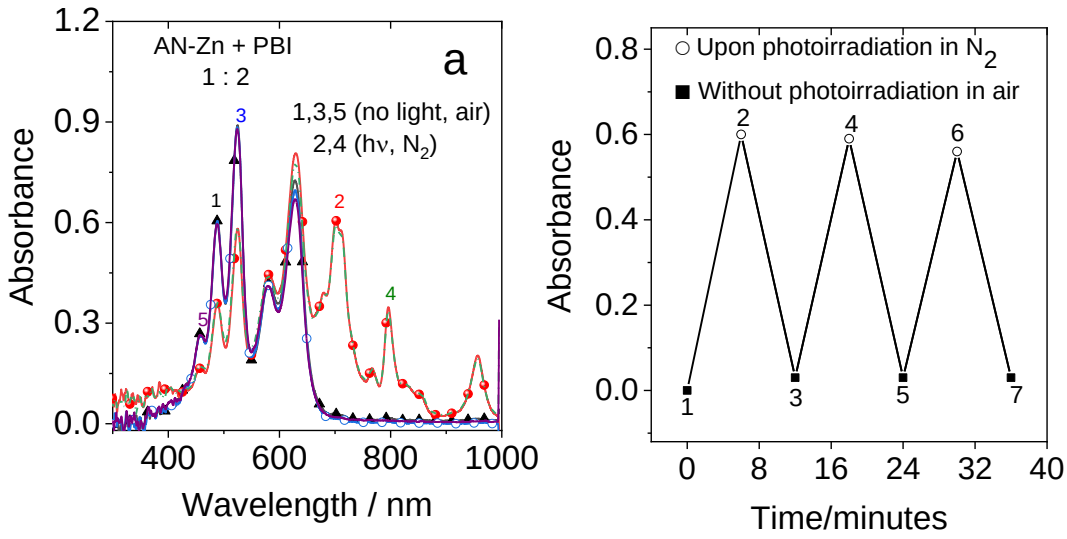

Figure S25. UV/Vis absorption spectra of **AN-Zn** in the presence of PBI and TEA in the deaerated dimethylformamide upon photoirradiation with red light (power density: 60-70 mW/cm^{-2}), *c* (**AN-Zn)** = 5×10^{-6} M, *c* (**PBI)** = 1×10^{-5} M and, *c* (**TEA)** = 2×10^{-4} M 20 °C. Reversibility of the formation of PBI$^{\bullet-}$ on photoirradiation and re-exposure to air.

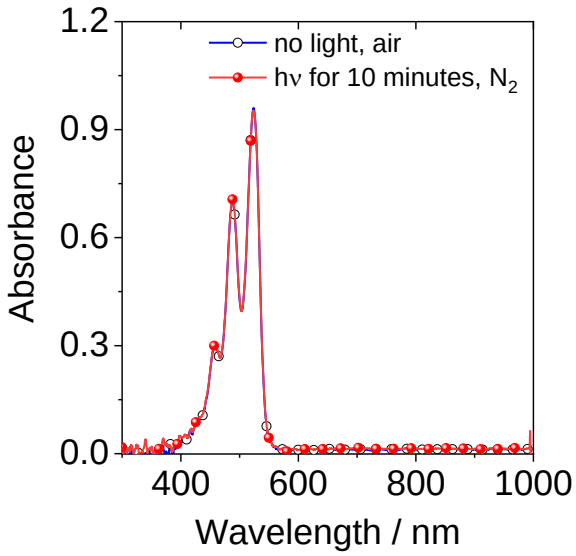

Figure S26. UV-Vis absorption spectra of **PBI** in the presence of TEA in the deaerated dimethylformamide upon photoirradiation with red light (power density: 60-70 mW/cm^{-2}) for 10 minutes, *c* (**PBI**) = 1×10^{-5} M and *c* (**TEA**) = 2×10^{-4} M, 20 °C.

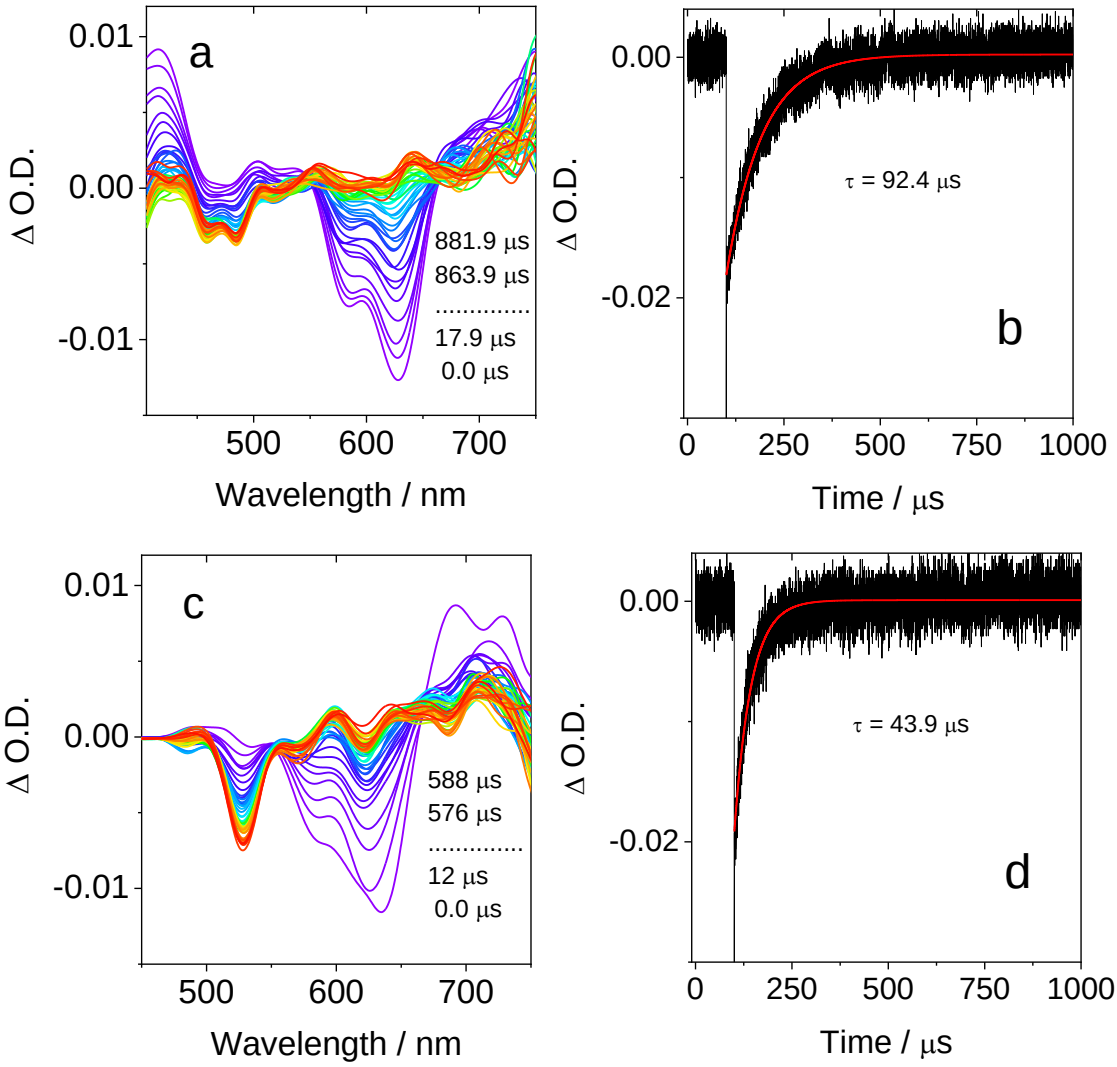

Figure S27. Nanosecond transient absorption spectra of (a) **AN-Zn**; and (b) **AN-Zn** + **PBI** (1:2) in deaerated dimethylformamide, upon ns pulsed laser excitation (λ_{ex} = 600 nm). Fig (b) and (d) are their respective decay curves at 630 nm, *c* (**AN-Zn**) = 5.0 × 10^{-6} M and *c* (**PBI**) = 1.0 × 10^{-5} M, 20 °C.

References

1. Z. Mahmood, N. Rehmat, S. Ji, J. Zhao, S. Sun, M. Di Donato, M. Li, M. Teddei and Y. Huo, *Chem. Eur. J.*, 2020, **26**, 14912−14918.
2. I. H. M. van Stokkum, D. S. Larsen and R. van Grondelle, *BBA - Bioenergetics*, 2004, **1657**, 82−104.
3. E. R. Henry and J. Hofrichter, in *Methods in Enzymol.*, 1992, **210**, 129−192.
4. J. Snellenburg, J., S. Laptenok, R. Seger, K. Mullen, M. and I. Van Stokkum, H.M., *J. Stat. Software*, 2012, **49(3)**, 1−22.
5. D. Tungulin, J. Leier, A. B. Carter, A. K. Powell, R. Q. Albuquerque, A. N. Unterreiner and C. Bizzarri, *Chem. Eur. J.*, 2019, **25**, 3816−3827.
6. R. Tabone, D. Feser, E. D. Lemma, U. Schepers and C. Bizzarri, *Front. Chem.*, 2021, **9**, 754420.
7. G. M. Miyake and J. C. Theriot, *Macromolecules*, 2014, **47**, 8255−8261.
8. N. Rehmat, I. V. Kurganskii, Z. Mahmood, Q. L. Guan, J. Zhao, Y. H. Xing, G. G. Gurzadyan and M. V. Fedin, *Chem. Eur. J.*, 2021, **27**, 5521−5535.